DIRECT STEAM CONDENSATION MODELING FOR A PASSIVE PWR SAFETY SYSTEM

D. R. Shaver[1*], S. P. Antal[1], M. Z. Podowski[1], D. H. Kim[2]

[1] *Rensselaer Polytechnic Institute, Troy, New York, USA*
[2] *Korean Atomic Energy Research Institute, Daejeon, Korea*
(*) corresponding author
shaved@rpi.edu, antals@rpi.edu, podowm@rpi.edu, dhkim8@kaeri.re.kr

Abstract

Due to the high effectiveness of direct steam condensation, it is being considered for use as a passive safety system in the design of a next generation 1400 MWe PWR, the APR1400. In order to gain an understanding of the physical principles governing direct condensation in a high speed steam jet, two independent models have been developed, cross compared, and validated with experimental data (Kim 2001). The first, a simplified model, uses a combination of the Lagrangian and Eulerian frames of reference to analyze the hydrodynamic behavior of liquid droplets present in the steam jet as well as predict the rate of condensation on a typical droplet. The second is a more complex computational multifield fluid dynamics model (CMFD) implemented in the state-of-the-art computer code NPHASE-CMFD. The simplified model is calibrated to experimental data and the results are used to generate boundary conditions for the CMFD model. Also, a condensation heat transfer model developed in the Lagrangian frame of reference in the simplified model has been translated into the Eulerian perspective for use with the CMFD model. It is shown that the predicted droplet concentration profiles, centerline temperature of the jet, and overall steam condensation rate are consistent with experimental observations.

1. INTRODUCTION

A passive safety system which vents steam into the in-containment refueling water storage tank (IRWST) is being considered in the design of a Korean advanced pressurized water reactor (APR1400). In the past, a similar concept has been used in BWRs, but it is a novel approach as applied to PWRs (Moon, 2009). The high effectiveness of direct steam condensation allows for a significant risk reduction of containment failure in the case of a LOCA. However, because of the intricacies of the interaction between a steam jet and the surrounding water, significant combined experimental, theoretical and computational research is needed to understand the underlying governing principles.

CMFD is an important tool in the field of nuclear reactor safety analyses. With the ever growing capabilities of modern computers, it is becoming possible to simulate complex interfacial phenomena, such as direct condensation of a high speed steam jet in a pool of subcooled water. The objective of this paper is to present and discuss theoretical and computational modeling concepts in an effort to produce a consistent method for analyzing direct steam condensation, as well as to compare the results of predictions to available experimental data.

In the evidence presented by Kim (2001), instabilities in the steam-water interface were observed to cause local atomization of the liquid phase, producing microscopic sized droplets. These droplets are ejected from the interface and travel throughout the jet. Understanding the interaction between the steam and the droplets is the key to analyzing the behavior of the jet. Two independent models have been developed for this purpose.

The first is a simplified, theoretical model which uses the combined Eulerian and Lagrangian systems of reference to follow droplets as they move through the jet. Heat transfer to a droplet is a transient phenomenon which strongly depends on the time the droplet is exposed to steam, and is weakly dependent on the specific path of the droplet through the flow. This process is dominated by the latent

heat released by the condensing steam. The Lagrangian frame of reference allows one to obtain a rigorous solution for the time dependent temperature profile inside a droplet to predict the rate of condensation on the droplet surface, the rate at which the droplet heats up, and the rate of growth of the droplet. The simplified model then solves the momentum and energy balance equations for individual droplets in the Lagrangian system of reference and translates the results into the Eulerian system of reference. This provides a description of the flow in the Eulerian perspective, which can be compared to a detailed CMFD model. The simplified model was used to parametrically study the effects of different droplet sizes and the velocity at which droplets enter the jet. This model has been calibrated against the experiment in order to provide reasonable boundary conditions for the CMFD simulation.

The second is a more complex CMFD model which has been implemented in the state-of-the-art computer code, NPHASE-CMFD (Tiwari, 2006). Since the simplified model does not predict the effect of the droplets on steam flow conditions, a complete CMFD model is necessary to capture the underlying local phenomena. The NPHASE-CMFD code solves the individual transport equations for mass and momentum, coupled or uncoupled; energy; and k and ε turbulence quantities individually for the continuous steam and dispersed droplet fields. It has been designed from the ground up as a multiphase/multicomponent solver and seamlessly handles the interactions between various phases. The code works with both structured and unstructured grids (Gallaway, 2009). Through the use of additional user routines, the code can be customized to handle specific problems, such as condensation mass transfer. The formulation of the governing equations is based on the ensemble-averaging concept (Podowski, 2009). Phenomena modeled by the CMFD model include the entrainment of droplets by the jet, interfacial forces between the droplets and the steam jet, condensation heat transfer from the steam to the droplets, as well as the effects of local velocity fields and droplet concentrations. This study uses the coupled mass/momentum solver, with the k-ε turbulence model for the steam phase. The results obtained from the CMFD simulations have been compared to those obtained from the simplified model, and both have been validated against the experimental data of Kim et al (2001).

2. OVERVIEW OF EXPERIMENTAL RESULTS

The Advanced 1400 MWe Power Reactor (APR1400) is scheduled to be in commercial operation in Korea by the mid 2010s. The new design features include four mechanically independent trains for the safety injection system with a Direct Vessel Injections (DVI) mode. Each of the four SITs has a fluidic device which passively controls the discharge rate into the reactor coolant system during the refill and the reflood phases. The benefit of the fluidic device is the elimination of the LPSI (low pressure injection system) pump from the safety injection system. The in-containment water storage (IW) system in the APR1400 consists of the IRWST, the holdup volume tank (HVT) and the cavity flooding system (CFS). The IRWST, which is an annular tank in the lower part of the containment, is designed to be used as a water source for the cavity flooding and the containment spray systems and also as a discharge location for the primary system's safety bleed operation. As the hydrogen generated from the reactor core is blown to the IRWST through the pressurizer, the hydrogen–steam behavior in the IRWST during a hypothetical severe accident is very important in the APR1400 containment in terms of steam condensation, hydrogen flame acceleration and DDT (deflagration detonation transient) in the IRWST. During the accident, water discharged from breaks of the RCS boundary and from the containment sprays is collected in the HVT and flows back into the IRWST when its level reaches the IRWST spillways. The APR1400 adopts an IVR-ERVC (in-vessel retention ex-vessel cooling) strategy for severe accident management aiming to preserve reactor vessel integrity. The CFS is designed to provide water to the reactor cavity from the IRWST. In addition, PARs are installed in the containment as hydrogen mitigation features in the APR1400. PAR is known as a passive and very effective long-term hydrogen removal system, though it may encounter limitations in the case of a large, instantaneous release.

The experimental study of Kim et al (2001) on direct contact condensation of a stable steam jet discharging into a quenching tank with cold water has been used as a reference point in the development and validation of the presented models. The objective of this study was to take measurements of direct

contact condensation of a stable steam jet discharging into a quenching tank filled with cold water. As seen in Fig. 1, the test facility used to observe steam jet condensation in a liquid pool consisted of a steam generator, a quench tank, a drain line, a coolant supply line, a steam supply line, a preheat line, valves, and the necessary instruments. The steam generator's maximum operating pressure was 1.03 MPa, and the maximum steam flow rate was 1000 kg/hr. The system produced a steady flow of steam at a quality higher than 99 %. The horizontal quenching tank was open to the atmosphere, and its diameter and length were 1 m and 1.5 m, respectively.

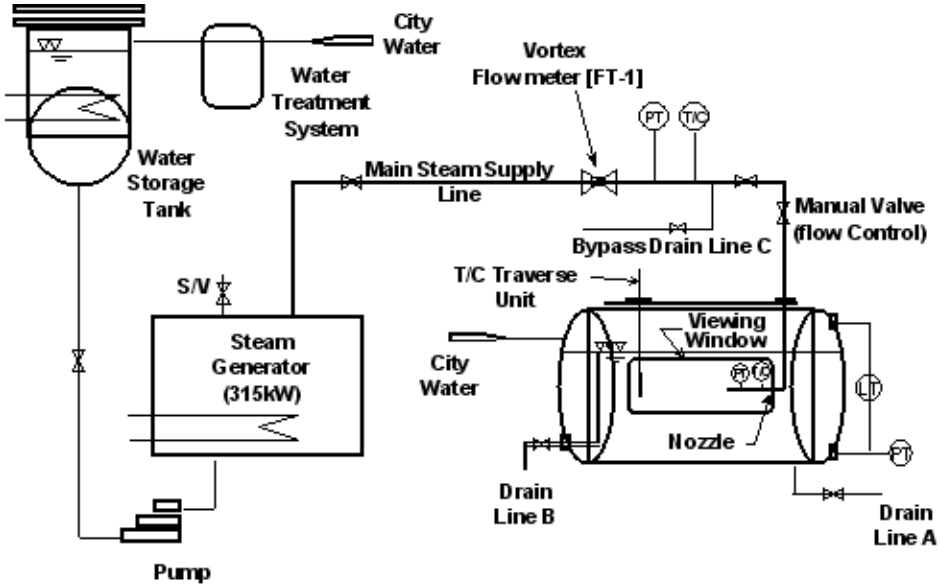

Fig. 1: Diagram of the experimental test facility (Kim, 2001)

Throughout the experiments, two steam jet shapes were typically observed. A conical shape of the steam jet was always observed for the 20 mm nozzle and an ellipsoidal shape was always observed for the 5 mm nozzle. Two typical results are shown in Fig. 2. For the nozzles between 5 and 20 mm, both jet shapes could be observed depending on the steam mass flux and pool temperature. Both shapes were stable in view of their condensation mode since the steam-water interface was relatively clear. Also, the steam jet expansion ratios, the dimensionless steam jet lengths and the average heat transfer coefficients were determined as functions of the steam mass flux and pool temperature.

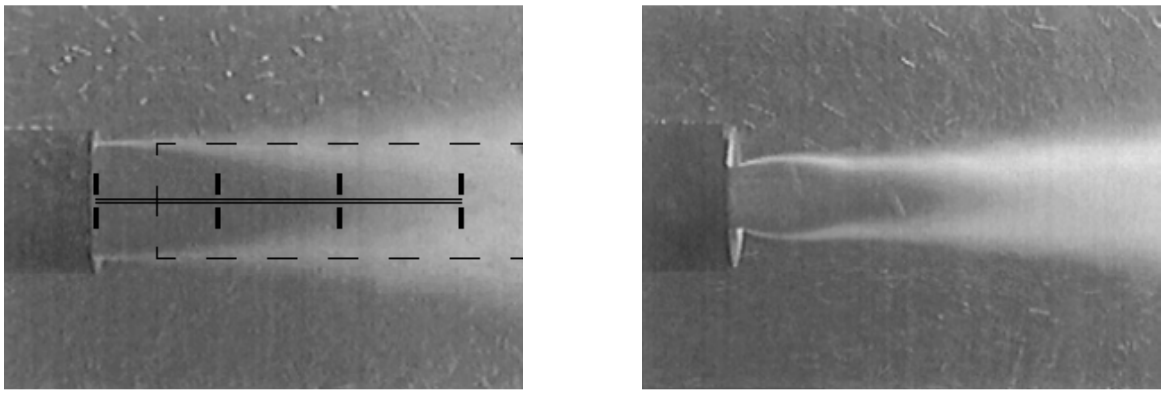

(a) (b)

Fig. 2: Photographs of the steam jet (Kim, 2001): (a) conical shape jet, (b) ellipsoidal shape jet. Distance marked at 20mm intervals. The dashed line indicates the analysis domain used in this paper.

Typical K-type thermocouples were used to measure the temperature distribution inside the two phase jet. The expected bias error from these instruments was +/- 1.5 °C. The measurements were taken several times at each location, and the associated statistical errors were practically negligible compared to the instrument errors. The locations of the thermocouples were initially set to the desired positions with a high accuracy. At the conclusion of the experiments, these locations were measured again and no displacements were observed. Therefore, it was concluded that the location errors were also negligible.

Typical measured temperature distributions in the steam jet and in the surrounding pool water are shown in Fig. 3 for four different pool temperatures. As can be seen in this figure, the centerline temperatures inside the steam cone did not change initially, and then dropped rather sharply at a distance of 10mm from the inlet.

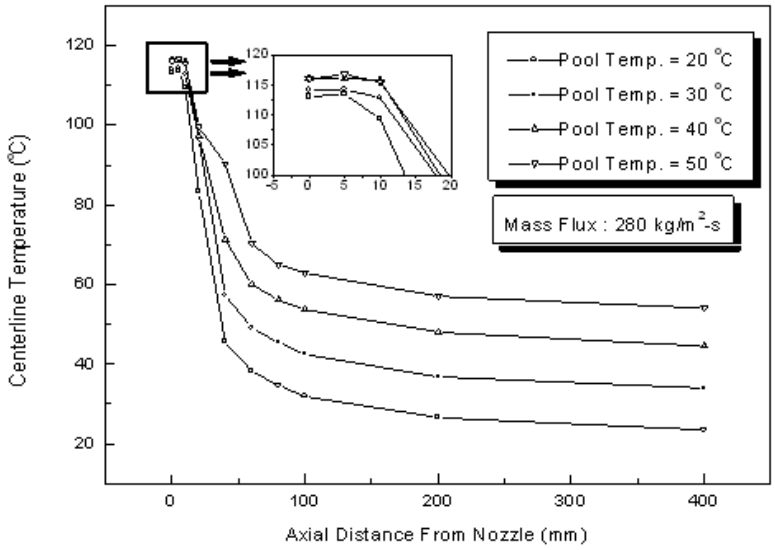

Fig. 3: Temperature measurements of the two-phase mixture at the centerline of the jet (Kim, 2001).

3. SIMPLIFIED, THEORETICAL MODEL FORMULATION

The rationale behind the development of a two-dimensional model was to gain insight into the physical phenomena governing the interaction between liquid droplets and condensing steam based on purely theoretical considerations. The model follows the progression of individual droplets through the steam jet. The domain used to model the steam jet is taken as a 2 cm wide, 10 cm long channel. This is represented by the dashed line in Fig. 2a, which overlays the domain on the actual steam jet.

Due to the high speed of the steam jet, the dominant force acting on the droplets within the domain is drag. It is expected that the turbulent breakup of the steam/liquid interface will produce droplets with initial velocities covering a large spectrum of values. The total population of the newly born droplets thus has been divided into several groups with each corresponding to a different velocity at injection. Each group is simulated individually and the cumulative local droplet concentration can be determined by adding together the contributions from each group of droplets.

The equations of motion for each group of droplets in the axial (x, u) and lateral (y, v) directions have been obtained from the corresponding force balance.

$$\frac{du}{dt} = -\frac{3}{4}\frac{C_d \rho_g U_{mag}}{\rho_f D}\left(u - U_{jet}\right) \tag{1}$$

$$\frac{dv}{dt} = -\frac{3}{4}\frac{C_d \rho_g U_{mag}}{\rho_f D} v \tag{2}$$

Here, $u(0) = u_0$ and $v(0) = v_0$ are the initial droplet velocities at injection and u_0 varies with different droplet groups.

The drag coefficient has been determined from a standard model for small spherical particles, as a function of the relative Reynolds number. In general, these equations must be solved numerically in order to account for the effects of increasing droplet diameter due to condensation, as well as of changing drag coefficient. However, based on test calculations it has been found that due to a short distance covered by the droplets and high liquid-to-steam density ratio, the increase in droplet diameter is minimal and the drag coefficient is inversely proportional to the droplet Reynolds number. This, in turn, allows for obtaining an analytic solution for the velocity components in the Lagrangian frame of reference

$$\frac{u(t) - U_{jet}}{u_0 - U_{jet}} = \exp\left(-\frac{3}{4}\frac{K_d \mu_g}{D^2 \rho_f} t \right) \tag{3}$$

$$\frac{v(t)}{v_0} = \exp\left(-\frac{3}{4}\frac{K_d \mu_g}{D^2 \rho_f} t \right) \tag{4}$$

By converting Eqs.(3) and (4) into the stationary (Eulerian) frame of reference, both velocity components can be expressed as functions of position across the steam jet.

$$\frac{u(y) - U_{jet}}{u_0 - U_{jet}} = 1 - \frac{3}{4}\frac{K_d \mu_g}{D^2 \rho_f}\frac{(y - y_0)}{v_0} \tag{5}$$

$$\frac{v(y)}{v_0} = 1 - \frac{3}{4}\frac{K_d \mu_g}{D^2 \rho_f}\frac{(y - y_0)}{v_0} \tag{6}$$

Because all droplets start from the same boundary, these equations are therefore valid for all droplets of a given field.

Interestingly, both velocity components vary linearly with the transverse coordinate. Due to the small diameter of the steam jet and the high velocities associated with the droplets, it is expected that they will be unable to slow down significantly within the jet domain and their traced paths will be nearly linear.

With the velocity components and boundary conditions independent of the axial coordinate, it follows that the concentration of droplets in each group should also be independent. The superficial velocity of the droplets in the transverse direction must then remain constant if mass transfer due to condensation is neglected. Using the expression for the velocity distribution in the lateral direction, the volume fraction across the jet can be found

$$\alpha = \frac{j_0}{v_0 - \frac{3}{4}\frac{K_d \mu_g}{D^2 \rho_f}(y - y_0)} \tag{7}$$

It is important to notice that the results shown above are based on several simplifying assumptions. However, many of these assumptions can be readily removed at the expense of losing the clarity of an analytic solution but with no significant impact on the solution accuracy. Thus, the results of predictions shown in the last section of the paper have been obtained by numerically solving Eqs. (1), (2) and (7) for a variable droplet diameter and a rigorous model of drag coefficient. Then, to determine the rate of droplet size change along the flow, the kinematic part of the model has been coupled with the steam/droplet interfacial heat transfer model.

The direct-contact energy transport between condensing steam and subcooled liquid droplets is due to two mechanisms: latent heat released due to condensation and heat conduction inside the droplets. A single

water droplet can be modeled as a sphere surrounded by a thin interface at the saturation temperature. The energy equation for the droplet including the interface is

$$\frac{d}{dt}\left(m_d h_d\right) = q_s - h_g \frac{dm_s}{dt} \tag{8}$$

where q_s is the convective heat transfer rate from the steam to the interface. If only the droplet without the interface is considered, the energy equation becomes

$$\frac{d}{dt}\left(m_d h_d\right) = q_d + h_f \frac{dm_d}{dt} \tag{9}$$

where q_d is the conductive heat transfer rate from the interface into the droplet. After rearranging, the heat transfer equation at the interface between the condensing steam and a liquid droplet becomes

$$q_s - h_g \frac{dm_s}{dt} = q_d + h_f \frac{dm_d}{dt} \tag{10}$$

where

$$\frac{dm_d}{dt} = -\frac{dm_s}{dt} = \Gamma_{s-d} \tag{11}$$

is the steam condensation rate. Since in the present case, steam superheat can be ignored, Eq.(10) simplifies to

$$h_{fg} \frac{dm_d}{dt} = q_d = A_d q''_d \tag{12}$$

where $A_d = \pi D_d^2$ is the droplet surface area and q''_d is the heat flux due to conduction inside the droplet volume.

From the Fourier law, the heat flux into the droplet can be modeled

$$q''_d = k_f \left.\frac{\partial T(r,t)}{\partial r}\right|_R \tag{13}$$

For spherical droplets, the radially-dependent droplet temperature is given by the heat conduction equation in spherical coordinates

$$\frac{1}{\alpha_f}\frac{\partial T}{\partial t} = \frac{1}{r^2}\frac{\partial}{\partial r}\left(r^2 \frac{\partial T}{\partial r}\right) \tag{14}$$

Where α_f is the thermal diffusivity of the droplets. Defining the dimensionless variables as

$$\theta = \frac{T - T_s}{T_i - T_s} \tag{15}$$

$$r^* = \frac{r}{R} \tag{16}$$

Eq.(14) with the appropriate boundary conditions yields the following solution

$$\theta\left(r^*, Fo\right) = \sum_{n=1}^{\infty} \frac{4\left(\sin\left(\lambda_n\right) - \lambda_n \cos\left(\lambda_n\right)\right)}{2\lambda_n - \sin\left(2\lambda_n\right)} \exp\left(-\lambda_n{}^2 Fo\right) \frac{\sin\left(\lambda_n r^*\right)}{\lambda_n r^*} \tag{17}$$

where the coefficients, λ_n, are given as the roots of

$$1 - \lambda_n \cot\left(\lambda_n\right) = Bi \tag{18}$$

and $Fo = \frac{\alpha_f t}{R^2}$ and $Bi = \frac{H_{eq} D_d}{2k}$ are the Fourier and Biot numbers respectively.

Rigorously speaking, Eq.(17) has been obtained for constant-diameter spheres. However, because the change in droplet diameter due to condensation is very small, it is still applicable to the current situation. Since the interface between a droplet and the steam is assumed to have a constant temperature

$$Bi = \infty \tag{19}$$

and the roots of Eq.(18) become

$$\lambda_n = n\pi \tag{20}$$

Consequently, Eq.(17) simplifies to

$$\theta\left(r^*, Fo\right) = \sum_{n=1}^{\infty} -2\cos\left(\lambda_n\right)\exp\left(-\lambda_n{}^2 Fo\right)\frac{\sin\left(\lambda_n r^*\right)}{\lambda_n r^*} \tag{21}$$

Differentiating Eq.(21) with respect to r^*

$$\frac{\partial\theta\left(r^*, Fo\right)}{\partial r^*} = \sum_{n=1}^{\infty} 2\cos\left(\lambda_n\right)\exp\left(-\lambda_n{}^2 Fo\right)\left[\frac{\sin\left(\lambda_n r^*\right)}{\lambda_n r^{*2}} - \frac{\cos\left(\lambda_n r^*\right)}{r^*}\right] \tag{22}$$

yields the following expression for the temperature gradient at the surface of the droplet

$$\left.\frac{\partial\theta\left(r^*, Fo\right)}{\partial r^*}\right|_{r^*=1} = -2\sum_{n=1}^{\infty}\exp\left(-n^2\pi^2 Fo\right) \tag{23}$$

Converting Eq.(23) into a dimensional form and substituting into Eq.(13), the surface heat flux becomes

$$q''_d = k_f \frac{4}{D}\left(\frac{h_f - h_i}{c_{p,f}}\right)\sum_{n=1}^{\infty}\exp\left(-n^2\pi^2\frac{4\alpha_f t}{D^2}\right) \tag{24}$$

Fortunately, the series in Eq.(24) converges very fast, so that a relatively small number of terms are sufficient to obtain an accurate estimate of the heat flux.

For a given heat transfer rate, the time-dependent mass of a droplet can be determined from the rate of condensation

$$m_d\left(t\right) = \rho_f \frac{\pi}{6} D^3 = \int_0^t \Gamma_{s-d}\left(t'\right)dt' + m_0 \tag{25}$$

The time-dependent average enthalpy of a droplet was then found from Eq.(9). Since the hydrodynamic model predicts the location of droplets at any given time, the time-dependent temperature of individual droplets in the Lagrangian system can be readily converted into a position-dependent temperature of the groups of droplets in the Eulerian system of reference.

4. CMFD MODEL FORMULATION

The CMFD model relies on the same basic phenomenological models as the simplified model. However, the condensation model has been developed specifically for the Lagrangian perspective. In order to make use of it in the CMFD model, it must be translated into the Eulerian perspective.

Assuming that heat transfer is into the droplets at all times, for any given time a droplet will have a unique mean temperature. The temperature gradient at the surface of the droplet can then be expressed as a function of mean temperature rather than time and the heat flux into the droplet becomes

$$q''_d = k_f \frac{2}{D}\left(\frac{h_f - h_i}{c_{p,f}}\right)\left.\frac{\partial\theta(r^*,\theta_m)}{\partial r^*}\right|_{r^*=1} \tag{26}$$

The temperature gradient is found *a priori* and used as input to the CMFD model. It is plotted in Fig. 4 as a function of Fourier number and as a function of mean temperature. The complete multifield model of gas/droplet flow has been implemented in the NPHASE-CMFD code (Antal et al., 2000).

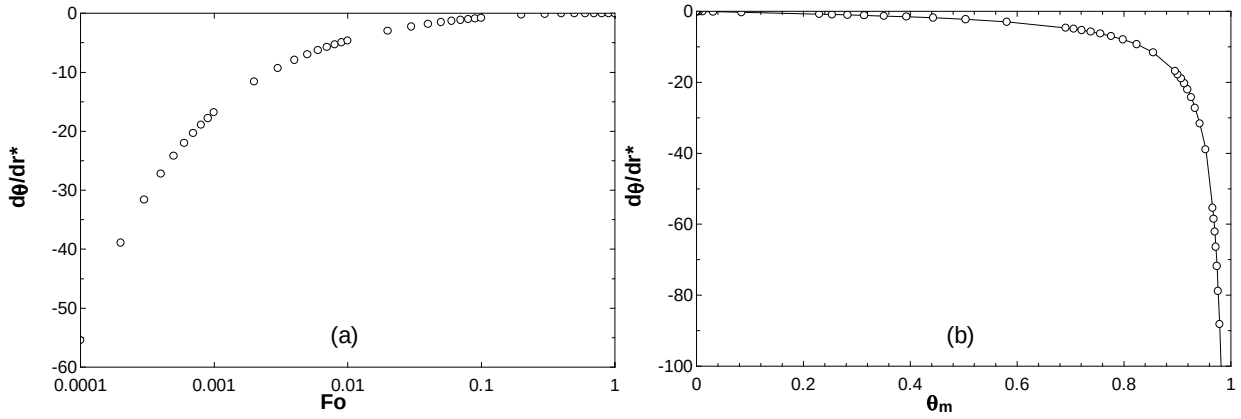

Fig. 4: Temperature gradient at the surface of a droplet as a function of (a) Fourier number and (b) mean droplet temperature.

5. RESULTS OF CALCULATIONS

In both models the total population of droplets has been divided into five groups. Based on extensive parametric testing on the effect of individual assumptions, the following boundary/initial conditions have been obtained for use in the final comparisons against data. Droplets 300 μm in diameter have been used, the initial droplet temperature has been prescribed equal to the water pool temperature (40 °C), and the transverse droplet injection velocity has been assumed to be 70 m/s.

In the simplified model, the steam velocity does not change and the initial droplet velocity in the axial direction remains constant. Conversely, the CMFD model is capable of capturing the effect of droplets on condensing steam. Thus, the corresponding boundary conditions have been modified, and the droplet axial velocities have been defined as fractions of the average steam velocity along the flow. For a constant steam velocity of 412 m/s, these boundary conditions would exactly match those used in the simplified model.

Since, due to the steam inlet superheat, condensation in the experiments starts at about 10 cm from the injection location, the inlet to the computational domain in the NPHASE-CMFD simulations has been shifted downstream from the nozzle by the same distance. This is shown in Fig. 2a. Because of the short distance from the jet injection opening, combined with a high steam velocity, a nearly-uniform steam velocity profile has been used at the inlet to the NPHASE-CMFD domain. Furthermore, to confirm the consistency of the jet inlet boundary conditions used in the simulation, the effect of the assumed jet velocity profile has been parametrically tested, from the 1/7 power law to uniform. It was observed that using the different profiles had no effect on the predictions of the steam condensation process.

To follow the best practice guidelines, a grid convergence study has been performed for the NPHASE-CMFD-based computational model. Specifically, the predictions obtained using two different grids have been compared against each other. First, a coarse grid, consisting of 25x25 elements was used. Then, the simulations were repeated using a fine grid consisting of 45x45 elements. Both grids are shown in Fig. 5,

and the corresponding results are presented in Fig. 6. As can be seen, the results for both meshes are very close to each other. Thus, it has been concluded that even the coarser grid produces, for all practical purposes, nearly-grid-independent predictions.

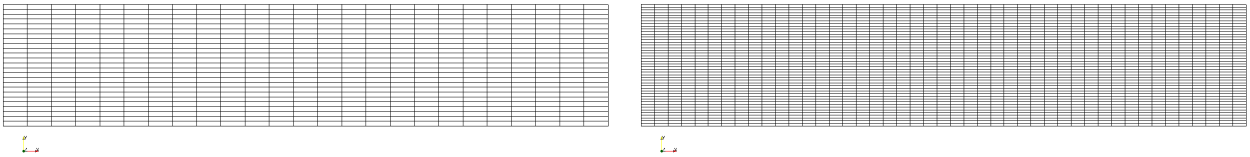

(a) (b)

Fig. 5: Grids used in the grid-independence study, (a) 25x25 coarse grid, (b) 45x45 fine grid.

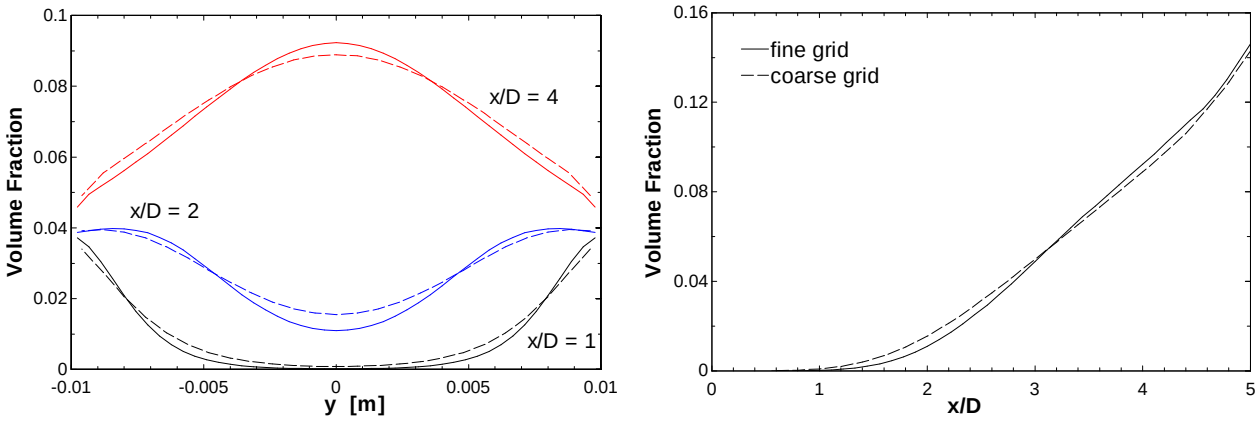

(a) (b)

Fig. 6: Comparison of the results for the fine and coarse grids, (a) droplet concentration across the jet and (b) local droplet concentration along the centerline of the jet. Solid lines indicate the fine grid; dashed lines indicate the coarse grid.

Fig. 7 shows the position-dependent droplet velocities for groups 1, 3 and 5. As can be seen, due to the short distance traveled across the jet and a high transverse injection velocity, the relative decrease in droplet velocity is only about 5%. The results obtained using the simplified model compare quite well against the NPHASE-CMFD predictions as well as to the analytical solution given by Eq. (6). Naturally, since the motion of droplets is axisymmetric, upon reaching the opposite wall, they deposit on the wavy surface of the liquid and/or get redirected back into the steam region.

The predicted lateral profiles of droplet concentration at an axial location equal to two jet diameters for the individual groups of droplets are shown in Fig. 8. Again, good agreement between the two models has been observed. Interestingly, the CMFD solution produces smoothed curves as compared to the step-function-like profiles produced by the simplified model.

Summing up the concentration for the individual groups yields the local droplet volume fraction as a function of both the distance from the center of the jet as well as from the steam injection zone. The lateral distributions of the cumulative droplet volume fraction at different axial locations along the steam flow are shown in Fig. 9. The observed trend shows an evolution of those profiles from wall-peaked to center-peaked.

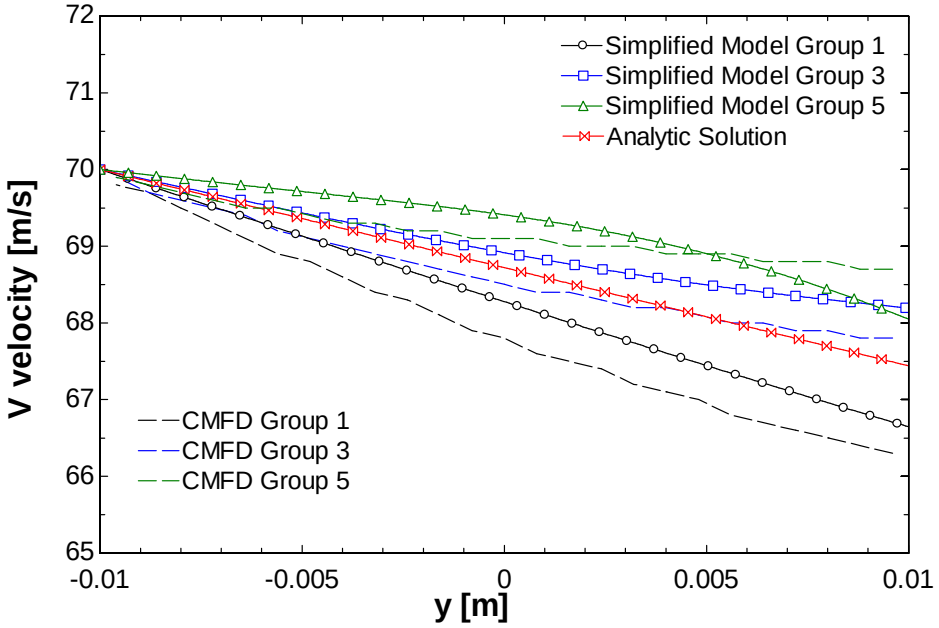

Fig. 7: Transverse component of velocity showing a comparison between the simplified model, the CMFD model, and the analytic solution given by Eq. (6).

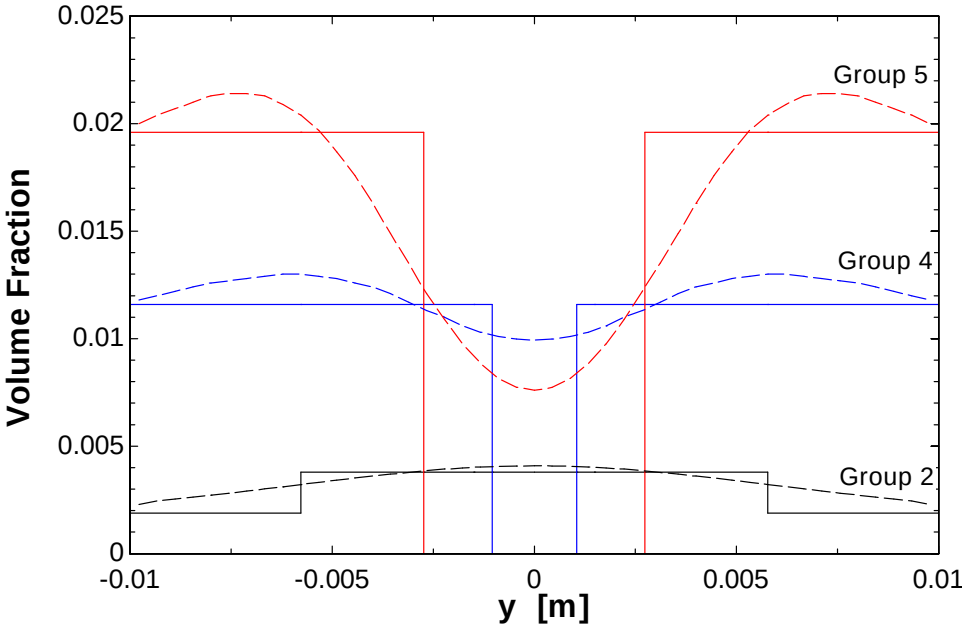

Fig. 8: Volume fraction profiles for individual droplet groups at $x/D = 2$. The simplified model's results are shown as solid lines and the CMFD model results are shown as dashed lines.

Based on the experimental evidence presented in Fig. 2 it is observed that the droplets moving through the steam jet create a visible cloud. From a comparison using the relative opacity of this cloud as an indicator of local droplet concentration, the general trends predicted by Fig. 9 are consistent with those observed in Fig. 2.

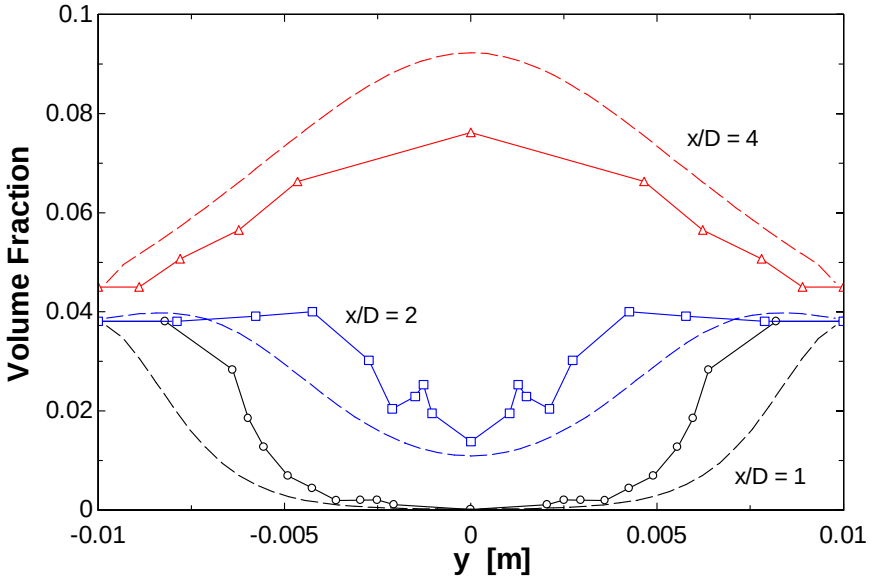

Fig. 9: Cumulative volume fraction profiles for droplets at various axial locations along the steam jet. The simplified model's results are shown as solid lines and the CMFD model results as dashed lines.

The profiles shown in Fig. 9 can be used to deduce the axial distributions of droplet volume fraction along the centerline, as well as the cross-sectional area averaged volume fraction along the channel. The corresponding plots are shown in Fig. 10. The results from the CMFD model are consistent with the simplified model for $x/D < 4$. After this location, the effects of decreasing steam velocity and increasing droplet concentration due to condensation become significant. The simplified model does account for these effects and the two models no longer agree.

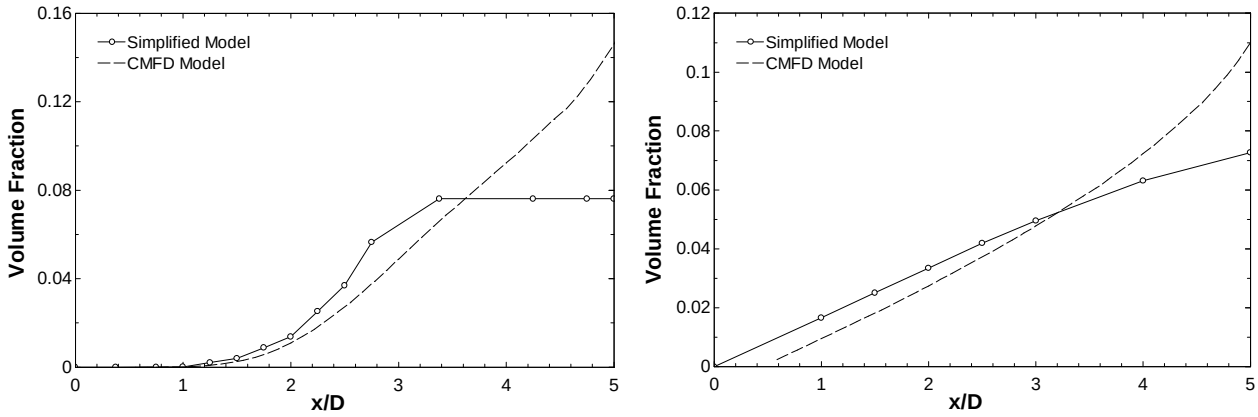

Fig. 10: Volume fraction of droplets along the jet, (a) at the centerline and (b) cross sectional averaged.

By assuming that the condensation rate for a single droplet in the simplified model is representative of the entire group, the total condensation rate in the steam jet can be estimated. In fact, the predicted distance downstream from the nozzle for complete steam condensation is around 3.75 jet diameters for the

simplified model and about 4.75 jet diameters for the CMFD model (see Fig. 11). Interestingly, the latter results agree quite well with the experimental observations.
The advantages of CMFD simulations can be clearly seen in Fig. 11, where complete contour plots of droplet volume fraction are shown. As it can be seen, the region near the end of the jet domain exhibits the greatest droplet concentration. Naturally, this region coincides with the region of a dramatic slow-down of steam and a decrease in the flow rate of uncondensed steam.

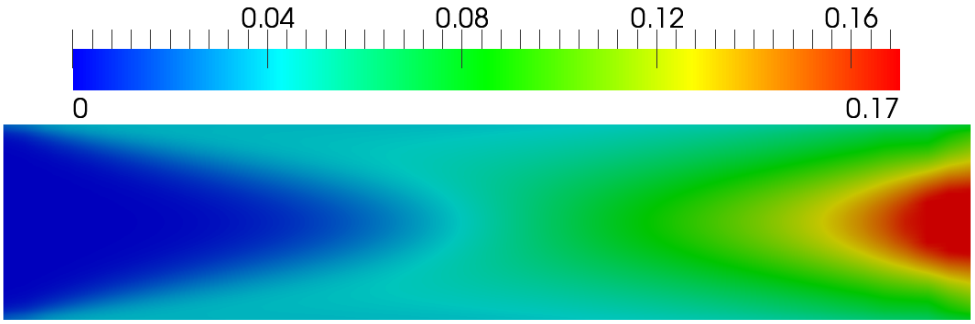

Fig. 11: CMFD predictions of local volume fraction within the steam jet (Shaver 2010)

One of the measured parameters in the experiments of Kim et al. (2001) was the average temperature of the steam/water mixture along the centerline of the jet. The measurements were performed using a thermocouple. This, in turn, indicates that for modeling purposes, the averaging concept should reflect the fractional average contact area between the micro-scale droplets and the thermocouple. Consequently, the following definition of the weighted-average temperature has been used in the present work

$$T = \frac{k_g T_g \left(1-\sum \alpha_n\right)^{\frac{2}{3}} + k_f T_l \left(\sum \alpha_n\right)^{\frac{2}{3}}}{k_g \left(1-\sum \alpha_n\right)^{\frac{2}{3}} + k_f \left(\sum \alpha_n\right)^{\frac{2}{3}}} \tag{27}$$

The definition given by Eq.(27) accounts for the effect of both thermal conductivities of each phase, as well as the volume fraction occupied by each phase. The two thirds exponent is used based on a weighting of the area-to-volume ratio, where the numerator of the exponent is a measure of the droplet-thermocouple contact area and the denominator is a measure of the droplet volume. This is consistent with the averaging done by Kim, Podowski and Antal (2008). In the CMFD model, another level of averaging has been used to account for the minor differences in the temperatures of droplets belonging to different groups. Combining the calculated droplet concentrations at the center line, shown in Fig. 10(a), with Eq.(27), the average steam/droplet temperature at the centerline has been evaluated for both the simplified model and the NPHASE-CMFD model The results are shown in Fig. 12.
As it can be seen, a good agreement between the predictions and the data has been obtained for both models. In particular, the trend in temperature change has been matched quite well. Some discrepancy is observed between the two models and the experimental data towards the end of the domain. In the simplified model, this is a result of the model's inability to account for local effects of condensation. The CMFD model continues to match the trend observed in the experimental data, but slightly under-predicts the measured temperature.

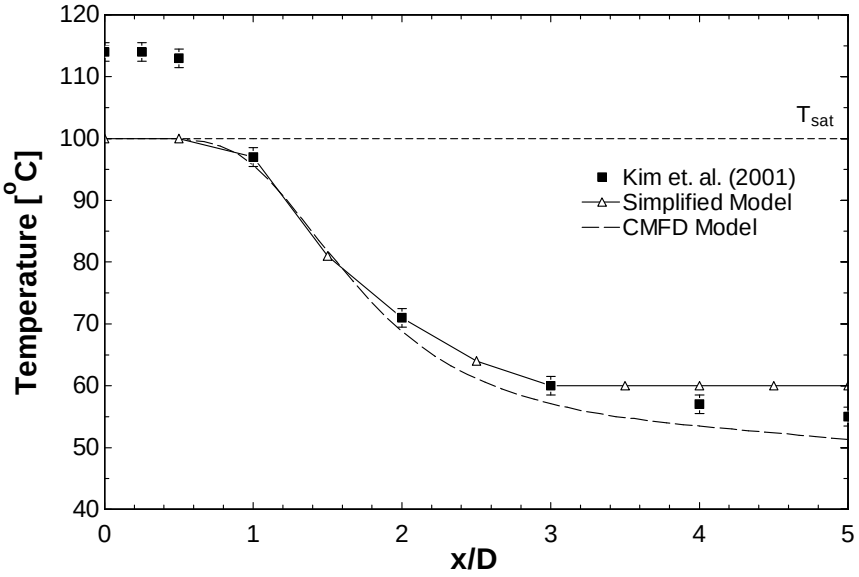

Fig. 12: A comparison between the experimental data and the results of simulations for the temperature of the two phase mixture along the centerline of the steam jet.

6. CONCLUSIONS

Two models of direct steam jet condensation in a large pool of liquid water have been developed: one is a simplified theoretical model, the other is a complete multidimensional model. The latter model has been implemented in the NPHASE-CMFD code. The results of predictions using both models have been compared against experimental data. Having the droplet diameter evaluating based on typical atomization criteria, the main adjustable parameter in both models was concerned with the initial velocity of droplets at injection into the condensing stem region.

It has been shown that the simplified model can predict the hydrodynamic behavior of droplets well, particularly along the initial 50-60% of the flow distance, where the effect of dispersed droplets on steam flow is negligible. On the other hand, the CMFD model properly predicts the effect of droplets on the steam along the entire flow path. This includes the cumulative distribution of droplets, as well as the overall condensation rate. Using the calibration assumptions mentioned above, good agreement has been observed in the NPHASE-CMFD-predicted condensation distance, the spatial distribution of droplets and the measured centerline temperature.

REFERENCES

Antal, S., Ettorre, S., Kunz, R. and Podowski, M., "Development of a next generation computer code for the prediction of multicomponent multiphase flows," Proceeding of the International Meeting on Trends in Numerical and Physical Modeling for Industrial Multiphase Flow, Cargese, France (2000).

T. Gallaway, S.P. Antal, M.Z. Podowski, "Mechanistic Multidimensional Analysis of Heat Transfer in Fluids at Supercritical Pressures", *Proc. International Congress on Advances in Nuclear Power Plants,* Tokyo, Japan, May 10-14, (2009).

D.H. Kim, M.Z. Podowski, S.P. Antal, "Modeling and Computer Simulation of High Speed Steam Jet Condensation in Cold Liquid Pool", Proc. 7th International Topical Meeting on Nuclear Reactor Thermal Hydraulics, Operation and Safety, Seoul, Korea, October 5-9, Paper 125 (2008).

H.Y. Kim et. al., "Experimental Study on the Stable Steam Condensation in a Quenching in a Quenching Tank", International Journal of Energy Research, 25, 239-252 (2001).

Y.T. Moon, H.D. Lee, G.C. Park, "CFD Simulation of Steam Jet-Induced Thermal Mixing in Subcooled Water Pool", Nuclear Engineering and Design, 239, 2849-2863 (2009).

M.Z. Podowski, "On the consistency of mechanistic multidimensional modeling of gas/liquid two-phase flows", Nuclear Engineering and Design, 239, 933–940 (2009).

D.R. Shaver, S.P. Antal, M.Z. Podowski, D.H. Kim, "Modeling and Analysis of Direct Steam Condensation in a Passive Safety System of Advanced PWR", Proc. 7th International Conference on Multiphase Flow, Tampa, FL, USA, May 30-June 4, (2010).

P. Tiwari, S.P. Antal, M.Z. Podowski, "Three-Dimensional Fluid Mechanics of Particulate Two-Phase Flows in U-Bend and Helical Conduits", Physics of Fluids, 18, 1-18 (2006).